Effect of the fabrication technique on the thermoelectric performance of Mg-based compounds—A case study of n-Type Mg2Ge

SANTOS, Rafael, DOU, Shi Xue, VASHAEE, Daryoosh and AMINORROAYA YAMINI, Sima <http://orcid.org/0000-0002-2312-8272>

Published version

SANTOS, Rafael, DOU, Shi Xue, VASHAEE, Daryoosh and AMINORROAYA YAMINI, Sima (2017). Effect of the fabrication technique on the thermoelectric performance of Mg-based compounds—A case study of n-Type Mg2Ge. ACS Omega, 2 (11), 8069-8074.

ACS OMEGA

Article

Cite This: ACS Omega 2017, 2, 8069-8074

http://pubs.acs.org/journal/acsodf

Effect of the Fabrication Technique on the Thermoelectric Performance of Mg-Based Compounds—A Case Study of n-Type Mg_2Ge

Rafael Santos,[†] Shi Xue Dou,[†] Daryoosh Vashaee,[‡] and Sima Aminorroaya Yamini*[,†,§]

[†]Australian Institute of Innovative Materials (AIIM), Innovation Campus, University of Wollongong, Squire Way, North Wollongong, New South Wales 2500, Australia

[‡]Electrical and Computer Engineering Department, North Carolina State University, Raleigh, North Carolina 27606, United States

[§]Department of Engineering and Mathematics, Sheffield Hallam University, City Campus, Sheffield S1 1WB, U.K.

Supporting Information

ABSTRACT: High performance, low cost, and low toxicity have been the main characteristics associated with magnesium-based thermoelectric materials. Nevertheless, the high volatility of magnesium creates challenges in the synthesis of these materials. In this work, n-type Mg_2Ge is synthesized using a solid-state technique, fully characterized, and compared with Mg_2Ge fabricated through different processes. We have found that Bi is an ineffective dopant in Mg_2Ge and precipitates into Mg_2Bi_3. Regardless of the technique used, the loss of Mg by evaporation and formation of precipitates in Bi-doped samples resulted in a low charge carrier concentration and, consequently, a low power factor. The precipitates significantly reduced the lattice thermal conductivity, however, leading to a figure-of-merit, zT, of 0.4 at 725 K, improving the previously reported figure-of-merit, zT, of 0.2 for Sb-doped Mg_2Ge. This work highlights the impact of the fabrication technique on the thermoelectric performance of Mg-based compounds.

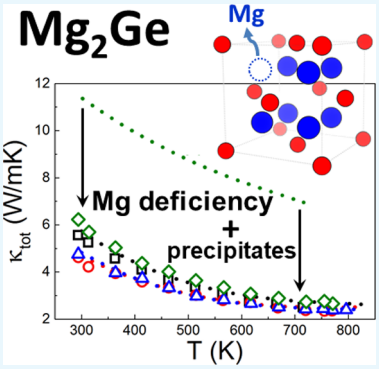

INTRODUCTION

Magnesium-based thermoelectric materials have garnered considerable attention because of their promising performance, low cost, and environmental friendliness.[1,2] Mg_2X (X = Si, Ge, and Sn) compounds crystallize in the $Fm3m$ space group, and they exhibit similar electronic band structures and a split conduction band. Recent studies have focused on the thermoelectric performance of n-type ternary[3−5] and quaternary[4,6,7] alloys of Mg_2Si, Mg_2Ge, and Mg_2Sn in various ratios to improve their conversion efficiency, defined by the figure-of-merit, $zT = S^2T/\rho\kappa_{tot}$, where S is the Seebeck coefficient, T is the absolute temperature, ρ is the electrical resistivity, and κ_{tot} is the total thermal conductivity, through the convergence of conduction bands[8,9] and increased mass-difference phonon scattering.[10−12] The binary compounds have received limited attention, however, because of their relatively low performances, especially Mg_2Ge, with three reports on n-type bulk samples[10,13,14] and only one report on the thin film p-type Mg_2Ge.[15] It is of great interest to understand the transport properties of these binary compounds and their interactions with the most common dopants to correctly design alloys with higher thermoelectric performance.

The fabrication of Mg-based semiconductors encounters intrinsic challenges because of the low vapor pressure and high reactivity of magnesium with potential crucibles. A large number of fabrication methods have been employed to synthesize Mg-based thermoelectric materials, including low-temperature ball milling,[8,16] solid-state reaction,[12,17] one-step sintering by spark plasma sintering (SPS) using MgH_2 as a precursor for Mg,[14,18] melting and casting using crucibles made of tantalum,[19] alumina sealed with B_2O_3,[20] boron nitride,[7] graphite,[12] and molybdenum foil[21] to avoid the reaction of magnesium with quartz, where these are sealed under vacuum. Here, we have synthesized n-type Mg_2Ge bulk samples by doping with Bi and Sb through the solid-state reaction. The transport properties of these samples are compared with those of previous studies,[10,13] including our recent report on n-type Mg_2Ge samples, fabricated via one-step SPS of elemental Ge and Bi/Sb with MgH_2.[14] A maximum zT of ∼0.4 at 725 K is achieved for $Mg_2Ge_{0.98}Bi_{0.02}$, an improvement over the zT of 0.2 for the Sb-doped Mg_2Ge[13] because of a significant decrease in the thermal conductivity, while obtaining a similar power factor (PF). Our work underscores the impact that different synthesis techniques have on the properties of Mg-based thermoelectrics and the difficulty in comparing these materials when they are synthesized by different methods.

RESULTS AND DISCUSSION

X-ray diffraction (XRD) patterns of the sintered $Mg_2Ge_{1-x}Bi_x$ (x = 0.01, 0.02, and 0.03) and $Mg_2Ge_{1-y}Sb_y$ (y = 0.02) samples (Figure 1) can be indexed to the cubic CaF_2 structure ($Fm3m$

Received: September 18, 2017
Accepted: November 7, 2017
Published: November 17, 2017

DOI: 10.1021/acsomega.7b01389
ACS Omega 2017, 2, 8069−8074

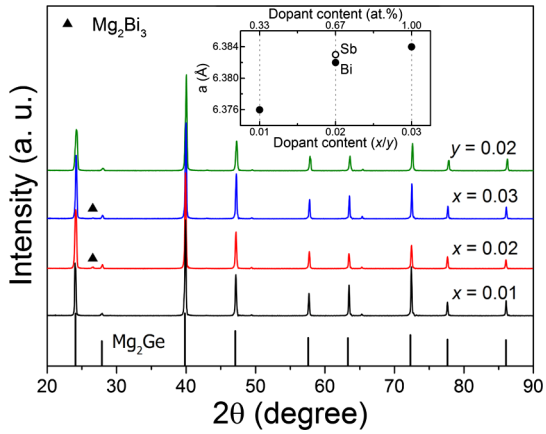

Figure 1. Room-temperature XRD patterns of $Mg_2Ge_{1-x}Bi_x$ (x = 0.01, 0.02, and 0.03) and $Mg_2Ge_{1-y}Sb_y$ (y = 0.02) samples. The inset shows the lattice parameter as a function of the dopant type and content, as obtained by Rietveld refinement. Trace amounts of Mg_2Bi_3 were detected in the Bi-doped samples with x = 0.02 and 0.03.

space group) of Mg_2Ge. Small amounts of the secondary phase Mg_2Bi_3 were detected in the Bi-doped samples with x = 0.02 and 0.03. The inset of Figure 1 shows the increase in the lattice parameter of Mg_2Ge with the increasing dopant concentration, as larger atoms of Bi and Sb substitute Ge atoms.[22] The difference between the lattice parameters of the samples with a Bi content of x = 0.02 and 0.03 is insignificant, which is consistent with the detection of Mg_2Bi_3 in these samples, suggesting that Bi added beyond 0.67 at. % has formed precipitates. The observed solubility of Bi in Mg_2Ge obtained in the current study using a solid-state synthesis technique is significantly higher than 0.17 at. % in our previous report, based on the one-step SPS synthesis of Mg_2Ge.[14] The latter method comprises a single step at a lower temperature that relies on the rapid reaction of Ge and MgH_2 upon hydrogen liberation, with an extremely short time for homogenization. The reaction of Mg with Bi also appears to have been preferred in the one-step SPS synthesis, reducing the amount of Bi available for doping. As the Mg_2Bi_3 precipitates were already formed, the subsequent annealing step had no effect beyond stabilization of the structure. In this work, the mixture was reacted in two stages at a higher temperature for a prolonged time, with grinding and homogenization of the powder in the interval between the stages, allowing for better dissolution of Bi in Mg_2Ge. Mg_2Bi_3 precipitates still formed, however, albeit only at higher concentrations of Bi.

The backscattered electron microscopy (BSE) images of both Bi- and Sb-doped samples at the same dopant concentration of x = 0.02 and y = 0.02 (0.67 at. %) confirmed the presence of precipitates with high atomic number at grain boundaries (particle size < 1 μm), which are indicated by arrows in Figure 2a, for the Bi-doped sample. The energy-dispersive spectroscopy (EDS) analysis (Figure 2c,d) reveals that these precipitates are rich in Bi, confirming the presence of the Mg_2Bi_3 phase detected by XRD. We have also detected that these precipitates in the Bi-doped samples are synthesized by a one-step SPS process.[14] The Sb-doped sample is free of precipitates (Figure 2b).

Temperature-dependent Seebeck coefficient (S), electrical resistivity (ρ), and PF, where PF = S^2/ρ, for $Mg_2Ge_{1-x}Bi_x$ (x = 0.01, 0.02, and 0.03) and $Mg_2Ge_{1-y}Sb_y$ (y = 0.02) samples are shown in Figure 3. All samples show a linear dependence of the Seebeck coefficient with a temperature of up to ~650 K, where it reaches a plateau (Figure 3a). Bi doping reduces the absolute S from ~210 μV/K for x = 0.01 to −190 μV/K for x = 0.02, after which it remains roughly constant, showing that further addition of Bi leads to an insignificant increase in the charge carrier concentration (Table 1), n, on which the position of the Fermi level and consequently the Seebeck coefficient are dependent. This result is consistent with the observation of Bi-rich precipitates formed at grain boundaries in the x = 0.02 sample. The Sb-doped sample exhibits a lower absolute S compared to the similarly Bi-doped samples, x = 0.02 and 0.03. The measured charge carrier concentrations of these samples are very similar (Table 1), indicating a comparable position of the Fermi level in relation to the bottom of the conduction band. According to eq 1

$$S = \frac{2k_B^2 T}{3e\hbar^2}\left(\frac{\pi}{3n}\right)^{2/3} m^*(1+r) \quad (1)$$

where k_B is the Boltzmann constant, e is the electron charge, $\hbar$ is the reduced Planck constant, m^* is the density of states

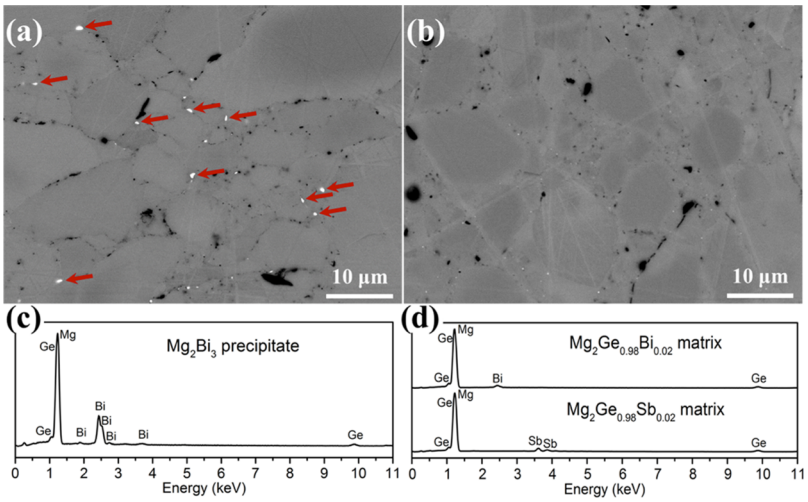

Figure 2. BSE images of $Mg_2Ge_{0.98}X_{0.02}$: (a) X = Bi and (b) X = Sb. Representative EDS spectra of (c) Mg_2Bi_3 precipitates (indicated by the arrows in (a)) and (d) $Mg_2Ge_{0.98}X_{0.02}$ (X = Bi and Sb).

DOI: 10.1021/acsomega.7b01389
ACS Omega 2017, 2, 8069−8074

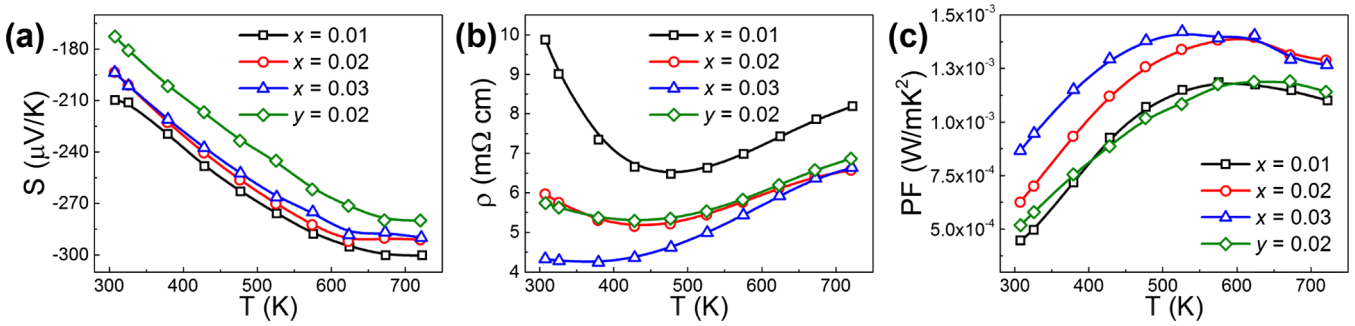

Figure 3. Temperature dependence of the (a) Seebeck coefficient, (b) electrical resistivity, and (c) PF of $Mg_2Ge_{1-x}Bi_x$ (x = 0.01, 0.02, and 0.03) and $Mg_2Ge_{1-y}Sb_y$ (y = 0.02).

Table 1. Room-Temperature Seebeck Coefficient, Electrical Resistivity, Hall Coefficient (R_H), Carrier Concentration (n), and Hall Mobility (μ_H)[a]

	S (μV/K)	ρ (mΩ·cm)	R_H (cm^3/C)	n (10^{18} cm^3)	μ_H (cm^2/V s)	z
Bi = 0.01	209.6	9.9	1.54	4.1	154	0.005
Bi = 0.02	193.6	5.9	0.92	6.8	154	0.010
Bi = 0.03	194.0	4.3	0.76	8.4	172	0.015
Sb = 0.02	148.7	5.7	0.78	8.0	136	0.010

[a]The final Mg deficiency, z, in $Mg_{2-z}Ge_{1-x}Bi_x$ (x = 0.01, 0.02, and 0.03) and $Mg_{2-z}Ge_{1-y}Sb_y$ (y = 0.02) was estimated based on the measured carrier concentration.

effective mass, and r is the scattering parameter.[23] Note that the Seebeck coefficient is proportional to $\frac{m^*(1+r)}{n^{2/3}}$. The carrier concentration values of samples doped with Bi and Sb are similar. Therefore, the difference in the Seebeck coefficient must arise from the differences in the effective mass, suggesting that Sb and Bi have different effects on the electronic band structure, as the scattering mechanism is unlikely to change between the dopants.

The electrical resistivity of the samples initially decreases with temperature, showing the typical behavior of intrinsic semiconductors, and exhibits metallic behavior at higher temperatures (Figure 3b). The magnitude and temperature of this behavioral change decrease with the dopant concentration, as the thermal energy needed to promote carriers to the conduction band decreases with the charge carrier concentration.[24] This effect is only visible because of the relatively low charge carrier concentrations in the current study, even at x = 0.03, as displayed in Figure 4, where a rapid decrease in the Hall coefficient (R_H) above ~200 K indicates the thermal excitation of electrons to the conduction band. The room-temperature Hall carrier mobility (Table 1), μ_H, has increased slightly by the addition of Bi. This is due to very low charge carrier concentrations of lightly doped samples, which show the behavior of transport properties of the nondegenerate semiconductor.

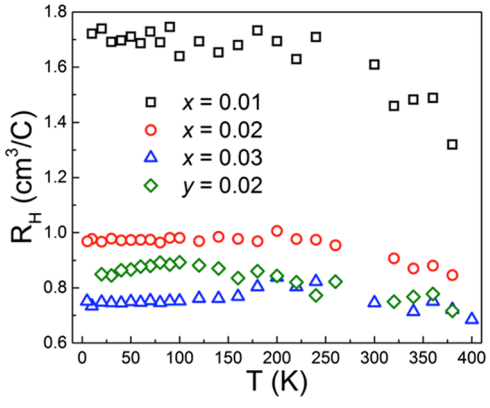

Figure 4. Temperature dependence of the Hall coefficient for $Mg_2Ge_{1-x}Bi_x$ (x = 0.01, 0.02, and 0.03) and $Mg_2Ge_{1-y}Sb_y$ (y = 0.02) samples.

The stoichiometry of Mg is known to have a significant effect on the electrical characteristics of Mg-based thermoelectric materials.[25] Each excess Mg atom occupies interstitial sites, contributing two electrons to the conduction band,[25] whereas each Mg atom vacancy acts either as a double hole donor[26,27] or as an electron trap localized within the band gap.[28] Regardless of the principle regulating Mg vacancies, Mg deficiency severely decreases the carrier concentration of n-type samples. This explains the much lower electron carrier concentration obtained in the current study, $n \approx 10^{18}$ cm^{-3}, compared to the similarly Sb-doped Mg_2Ge,[13] which resulted in a room-temperature electrical resistivity of 0.195 mΩ·cm and a carrier concentration of 5.8×10^{20} cm^{-3} for $Mg_{2.2}Ge_{0.99}Sb_{0.01}$ with excess Mg. The deficiency of Mg (z) in $Mg_{2-z}Ge_{1-x}Bi_x$ and $Mg_{2-z}Ge_{1-y}Sb_y$ was estimated using $z = \frac{1}{2}\left(\frac{V \times n}{4} - x\right)$, where V is the unit cell volume, n is the carrier concentration, and x is the dopant stoichiometry, and the results are displayed in Table 1. This equation estimates the Mg deficiency by considering Bi atoms and Mg vacancies as the only sources of charge carriers/vacancies in the system, that is, assuming that there are no Mg_2Bi_3 precipitates.

The bipolar effect is observed at temperatures above ~650 K in the Seebeck coefficient plot (Figure 3a), similar to our previous study.[14] This effect is not visible on the thermal conductivity plot as a function of temperature (Figure 5a) because of the negligible bipolar component of the thermal conductivity[29] (κ_b) (Figure S1 of the Supporting Information).

The total (κ_{tot}) and lattice (κ_{lat}) thermal conductivities of the samples are shown in Figure 5a. The Wiedemann–Franz relation, $\kappa_e = L_0 T/\rho$, is used to calculate the electronic thermal

DOI: 10.1021/acsomega.7b01389
ACS Omega 2017, 2, 8069−8074

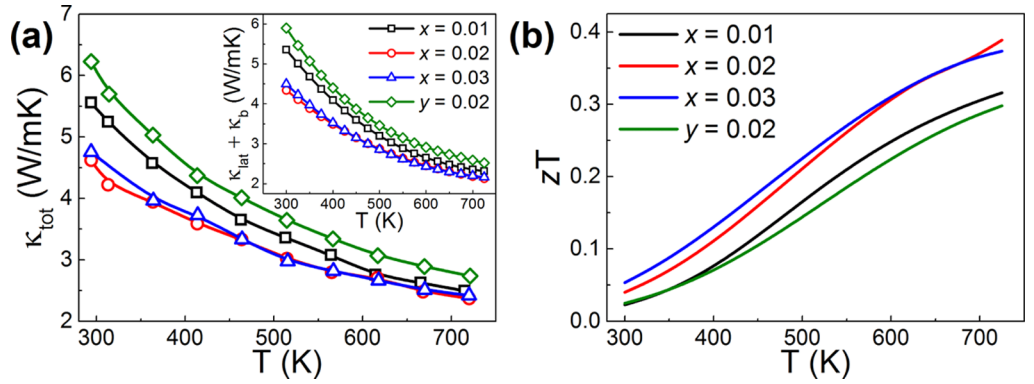

Figure 5. Temperature dependence of the (a) total thermal conductivity (with the sum of the lattice and bipolar components as an inset) and (b) figure-of-merit, zT, of $Mg_2Ge_{1-x}Bi_x$ and $Mg_2Ge_{1-y}Sb_y$.

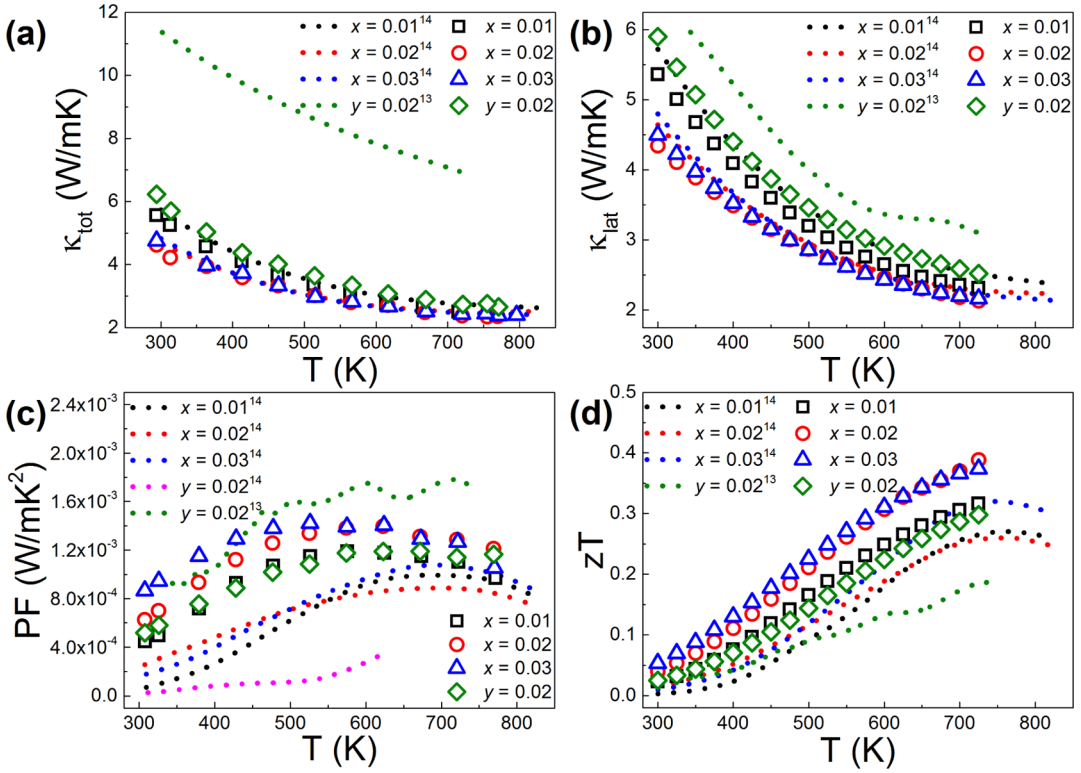

Figure 6. Temperature dependence of the (a) total thermal conductivity, (b) lattice component of the thermal conductivity, (c) PF, and (d) figure-of-merit, zT, of $Mg_2Ge_{1-x}Bi_x$ (x = 0.01, 0.02, and 0.03) and $Mg_2Ge_{1-y}Sb_y$ (y = 0.02) samples from this work compared with other reports on n-Mg_2Ge.[13,14]

conductivity, where L_0 is the Lorenz number and ρ is the electrical resistivity. The Lorenz number used in the calculation of κ_e is the theoretical limit for degenerate semiconductors 2.45 $\times$ 10^{-8} V^2 K^{-2}.[30] The lattice and bipolar thermal conductivities of all samples are calculated by deducting the electronic contribution to the total thermal conductivity using $\kappa_{tot} = \kappa_{lat} + \kappa_e + \kappa_b$ (Figure 5a inset). The lattice thermal conductivity dominates κ_{tot} in all samples, and it decreases with the temperature and Bi dopant concentration. Even though the charge carrier density increased slightly with the added dopant, the electronic component of the thermal conductivity is too small to significantly contribute to the total thermal conductivity.

The total thermal conductivity of the samples produced in the current study is much lower than that in the previous report on heavily doped n-Mg_2Ge[13] (Figure 6a). Figure 6b shows that the lattice thermal conductivity in the previous report is similar to that of the Sb-doped sample in the current study, which is evidence of the significantly lower contribution of the electronic thermal conductivity, originating from the low carrier concentration of our samples. The lattice thermal conductivity of the Bi-doped samples is lower than that of the Sb-doped one owing to the increased phonon scattering by Mg_2Bi_3 precipitates and point defects. Moreover, the effect of the precipitates is visible in the significant decrease in the lattice thermal conductivity with the increased Bi concentration. The formation of Mg_2Bi_3 leads to further depression of the electron concentration by reducing the amount of available Bi, which acts as an electron donor in Mg_2Ge, and by leading to the additional loss of Mg from the matrix. Furthermore, the low charge carrier concentration of the samples produced in this work makes κ_e practically negligible, representing only ~4% of

DOI: 10.1021/acsomega.7b01389
ACS Omega 2017, 2, 8069−8074

κ_{tot}, whereas in highly doped Mg_2Ge,[13] it accounts for ~50%. Despite the significantly higher electrical resistivity obtained in the previous report[14] and in this work, when compared to the heavily Sb-doped Mg_2Ge,[13] our samples exhibit a similar PF (Figure 6c). The final zT of our samples is therefore higher, owing to the reduced thermal conductivity (Figure 6d). These results suggest that studying the interaction of Bi with high zT Mg-based thermoelectrics alloyed with Ge might be of interest to improve our understanding of their high performance and perhaps guide further improvements. To take advantage of the impact of precipitates on the thermal conductivity while maintaining low electronic resistivity, we suggest a double-doping approach with Sb and Bi.

CONCLUSIONS

n-type Mg_2Ge bulk samples doped with Bi or Sb were synthesized via a solid-state reaction and compared with previous reports on n-type Mg_2Ge fabricated by different processes. Despite the attempt to compensate for the Mg loss in the current study, all samples exhibited deficiency of magnesium, heavily depressing the charge carrier concentration. Furthermore, Bi reacted with Mg to form Mg_2Bi_3 precipitates, leading to further Mg loss and reduced doping of Mg_2Ge by Bi. This led to a high electrical resistivity, a high Seebeck coefficient, and a low lattice thermal conductivity, whereas the electronic thermal conductivity was negligible. This resulted in a maximum zT of ~0.4 at 725 K for $Mg_2Ge_{0.98}Bi_{0.02}$. These results highlight the impact of the fabrication technique on the magnesium stoichiometry in Mg-based thermoelectric compounds and indicate that Bi is an unsuitable dopant for Mg_2Ge.

MATERIALS AND METHODS

Magnesium turnings (Mg, Alfa Aesar, 99.98%), germanium powder (Ge, Alfa Aesar, 99.999%), bismuth powder (Bi, Alfa Aesar, 99.999%), and antimony shots (Sb, Alfa Aesar, 99.999%) were used to synthesize $Mg_2Ge_{1-x}Bi_x$ (x = 0.01, 0.02, and 0.03) and $Mg_2Ge_{1-y}Sb_y$ (y = 0.02). Stoichiometric mixtures of elements were sealed in a boron nitride-coated vacuum-sealed quartz ampoule, with 50 wt % extra Mg to compensate for losses during the synthesis processes. The required amount of extra magnesium was optimized to obtain a single-phase compound, that is, free of unreacted Ge, as determined by the XRD analysis. This approach was necessary to directly compare the impact of different synthesis techniques on the characteristics of Mg_2Ge samples with added Bi and Sb. The mixtures were reacted at 1123 K for 30 min and annealed at 673 K for 10 h. The product was hand-ground to a fine powder in an agate mortar and pestle, and the resulting powders were sintered in a 12 mm graphite die using SPS at 1073 K and an axial pressure of 50 MPa for 1 h under vacuum. All material and powder handling and preparation were performed in a glovebox under a positive-pressure argon atmosphere.

The crystal structure and phase characterization were obtained with a MAC Science X-ray diffractometer with Cu Kα radiation (λ = 1.544 Å, 40 kV, 25 mA). The obtained powder XRD patterns were fitted using Rietveld refinement to estimate the lattice parameters of the synthesized samples. The microstructure and phase composition of the $Mg_2Ge_{1-x}Bi_x$ and $Mg_2Ge_{1-y}Bi_y$ samples were analyzed by a scanning electron microscopy (SEM; JEOL 7001F SEM) instrument, with the SEM equipped with EDS. The thermal diffusivity (D) was obtained using the laser flash method with a Linseis LFA 1000 instrument and used to calculate the thermal conductivity (κ), from $\kappa = d{\cdot}D{\cdot}C_p$. The density ($d$) was measured using dimensions and weight of the sample, whereas the heat capacity (C_p) was obtained from the literature.[8,31,32] The Seebeck coefficient (S) and the electrical conductivity (σ) were obtained using the slope method in a quasi-steady-state mode of a Linseis LSR-3 instrument, with temperature differences between the probes of 2−10 K in the parallelepiped-shaped samples. Hall effect measurements were performed using a Physical Property Measurement System from Quantum Design from 5 to 400 K.

ASSOCIATED CONTENT

Supporting Information

The Supporting Information is available free of charge on the ACS Publications website at DOI: 10.1021/acsomega.7b01389.

Lattice and bipolar conductivity as a function of inverse temperature (PDF)

AUTHOR INFORMATION

Corresponding Author

*E-mail: S.Aminorroaya@shu.ac.uk (S.A.Y.).

ORCID

Sima Aminorroaya Yamini: 0000-0002-2312-8272

Notes

The authors declare no competing financial interest.

ACKNOWLEDGMENTS

We would like to thank Australian Research Council (ARC)—LP120200289 and ARC Discovery Early Career Award DE130100310 for financial support.

REFERENCES

(1) LeBlanc, S.; Yee, S. K.; Scullin, M. L.; Dames, C.; Goodson, K. E. Material and manufacturing cost considerations for thermoelectrics. *Renewable Sustainable Energy Rev.* **2014**, *32*, 313−327.

(2) Zaitsev, V. K.; Fedorov, M. I.; Eremin, I. S.; Gurieva, E. A. Thermoelectrics on the Base of Solid Solutions of Mg_2B^{IV} Compounds (B^{IV}=Si, Ge, Sn). In *Thermoelectrics Handbook: Macro to Nano*; Rowe, D. M., Ed.; CRC Press: Boca Raton, FL, USA, 2006; Chapter 29.

(3) Zheng, L.; Zhang, X.; Liu, H.; Li, S.; Zhou, Z.; Lu, Q.; Zhang, J.; Zhang, F. Optimized nanostructure and thermoelectric performances of $Mg_2(Si_{0.4}Sn_{0.6})Sb_x$ solid solutions by in situ nanophase generation. *J. Alloys Compd.* **2016**, *671*, 452−457.

(4) Mao, J.; Kim, H. S.; Shuai, J.; Liu, Z.; He, R.; Saparamadu, U.; Tian, F.; Liu, W.; Ren, Z. Thermoelectric properties of materials near the band crossing line in Mg_2Sn−Mg_2Ge−Mg_2Si system. *Acta Mater.* **2016**, *103*, 633−642.

(5) Liu, W.; Zhou, J.; Jie, Q.; Li, Y.; Kim, H. S.; Bao, J.; Chen, G.; Ren, Z. New insight into the material parameter B to understand the enhanced thermoelectric performance of $Mg_2Sn_{1-x-y}Ge_xSb_y$. *Energy Environ. Sci.* **2016**, *9*, 530−539.

(6) Kutorasinski, K.; Tobola, J.; Kaprzyk, S.; Khan, A. U.; Kyratsi, T. Electronic Structure and Thermoelectric Properties of Pseudoquaternary $Mg_2Si_{1-x-y}Ge_y$-Based Materials. *J. Electron. Mater.* **2014**, *43*, 3831−3837.

(7) Yin, K.; Su, X.; Yan, Y.; You, Y.; Zhang, Q.; Uher, C.; Kanatzidis, M. G.; Tang, X. Optimization of the Electronic Band Structure and the Lattice Thermal Conductivity of Solid Solutions According to Simple Calculations: A Canonical Example of the $Mg_2Si_{1-x-y}Ge_xSn_y$ Ternary Solid Solution. *Chem. Mater.* **2016**, *28*, 5538−5548.

(8) Liu, W.; Kim, H. S.; Chen, S.; Jie, Q.; Lv, B.; Yao, M.; Ren, Z.; Opeil, C. P.; Wilson, S.; Chu, C.-W.; Ren, Z. n-type thermoelectric

DOI: 10.1021/acsomega.7b01389
ACS Omega 2017, 2, 8069−8074

material $Mg_2Sn_{0.75}Ge_{0.25}$ for high power generation. *Proc. Natl. Acad. Sci. U.S.A.* **2015**, *112*, 3269−3274.
(9) Zaitsev, V. K.; Fedorov, M. I.; Gurieva, E. A.; Eremin, I. S.; Konstantinov, P. P.; Samunin, A. Y.; Vedernikov, M. V. Highly effective $Mg_2Si_{1-x}Sn_x$ thermoelectrics. *Phys. Rev. B: Condens. Matter Mater. Phys.* **2006**, *74*, 045207.
(10) Nolas, G. S.; Wang, D.; Lin, X. Synthesis and low temperature transport properties of $Mg_2Ge_{1-y}Sb_y$. *Phys. Status Solidi RRL* **2007**, *1*, 223−225.
(11) Tani, J.-i.; Kido, H. Lattice dynamics of Mg_2Si and Mg_2Ge compounds from first-principles calculations. *Comput. Mater. Sci.* **2008**, *42*, 531−536.
(12) Vlachos, N.; Hatzikraniotis, E.; Mihailescu, C. N.; Giapintzakis, J.; Kyratsi, T. The Effect of Ge on $Mg_2Si_{0.6-x}Sn_{0.4}Ge_x$ Materials. *J. Electron. Mater.* **2014**, *43*, 3844−3851.
(13) Gao, H. L.; Zhu, T. J.; Zhao, X. B.; Deng, Y. Influence of Sb doping on thermoelectric properties of Mg_2Ge materials. *Intermetallics* **2015**, *56*, 33−36.
(14) Santos, R.; Nancarrow, M.; Dou, S. X.; Yamini, S. A. Thermoelectric performance of n-type Mg_2Ge. *Sci. Rep.* **2017**, *7*, 3988.
(15) Chuang, L.; Savvides, N.; Tan, T. T.; Li, S. Thermoelectric Properties of Ag-doped Mg_2Ge Thin Films Prepared by Magnetron Sputtering. *J. Electron. Mater.* **2009**, *39*, 1971−1974.
(16) Polymeris, G. S.; Vlachos, N.; Khan, A. U.; Hatzikraniotis, E.; Lioutas, C. B.; Delimitis, A.; Pavlidou, E.; Paraskevopoulos, K. M.; Kyratsi, T. Nanostructure and doping stimulated phase separation in high-ZT $Mg_2Si_{0.55}Sn_{0.4}Ge_{0.05}$ compounds. *Acta Mater.* **2015**, *83*, 285−293.
(17) Zhang, Q.; Zheng, Y.; Su, X.; Yin, K.; Tang, X.; Uher, C. Enhanced power factor of $Mg_2Si_{0.3}Sn_{0.7}$ synthesized by a non-equilibrium rapid solidification method. *Scr. Mater.* **2015**, *96*, 1−4.
(18) Chen, S.; Zhang, X.; Fan, W.; Yi, T.; Quach, D. V.; Bux, S.; Meng, Q.; Kauzlarich, S. M.; Munir, Z. A. One-step low temperature reactive consolidation of high purity nanocrystalline Mg_2Si. *J. Alloys Compd.* **2015**, *625*, 251−257.
(19) Farahi, N.; Prabhudev, S.; Botton, G. A.; Zhao, J.; Tse, J. S.; Liu, Z.; Salvador, J. R.; Kleinke, H. Local structure and thermoelectric properties of $Mg_2Si_{0.977-x}Ge_xBi_{0.023}$ ($0.1 \leq x \leq 0.4$). *J. Alloys Compd.* **2015**, *644*, 249−255.
(20) Gao, H.; Zhu, T.; Liu, X.; Chen, L.; Zhao, X. Flux synthesis and thermoelectric properties of eco-friendly Sb doped $Mg_2Si_{0.5}Sn_{0.5}$ solid solutions for energy harvesting. *J. Mater. Chem.* **2011**, *21*, 5933.
(21) Zhang, L.; Xiao, P.; Shi, L.; Henkelman, G.; Goodenough, J. B.; Zhou, J. Suppressing the bipolar contribution to the thermoelectric properties of $Mg_2Si_{0.4}Sn_{0.6}$ by Ge substitution. *J. Appl. Phys.* **2015**, *117*, 155103.
(22) Tani, J.-i.; Takahashi, M.; Kido, H. First-principles calculation of impurity doping into Mg_2Ge. *J. Alloys Compd.* **2009**, *485*, 764−768.
(23) Tang, Y.; Gibbs, Z. M.; Agapito, L. A.; Li, G.; Kim, H.-S.; Nardelli, M. B.; Curtarolo, S.; Snyder, G. J. Convergence of multi-valley bands as the electronic origin of high thermoelectric performance in CoSb3 skutterudites. *Nat. Mater.* **2015**, *14*, 1223−1228.
(24) Chien, C. L.; Westgate, C. R. *The Hall Effect and Its Applications*; Springer: New York, 1980.
(25) Du, Z.; Zhu, T.; Chen, Y.; He, J.; Gao, H.; Jiang, G.; Tritt, T. M.; Zhao, X. Roles of interstitial Mg in improving thermoelectric properties of Sb-doped $Mg_2Si_{0.4}Sn_{0.6}$ solid solutions. *J. Mater. Chem.* **2012**, *22*, 6838.
(26) Tobola, J.; Kaprzyk, S.; Scherrer, H. Mg-Vacancy-Induced Semiconducting Properties in $Mg_2Si_{1-x}Sb_x$ from Electronic Structure Calculations. *J. Electron. Mater.* **2009**, *39*, 2064−2069.
(27) Kato, A.; Yagi, T.; Fukusako, N. First-principles studies of intrinsic point defects in magnesium silicide. *J. Phys.: Condens. Matter* **2009**, *21*, 205801.
(28) Zhang, L.; Xiao, P.; Shi, L.; Henkelman, G.; Goodenough, J. B.; Zhou, J. Localized Mg-vacancy states in the thermoelectric material $Mg_{2-\delta}Si_{0.4}Sn_{0.6}$. *J. Appl. Phys.* **2016**, *119*, 085104.
(29) Zhao, L. D.; Wu, H. J.; Hao, S. Q.; Wu, C. I.; Zhou, X. Y.; Biswas, K.; He, J. Q.; Hogan, T. P.; Uher, C.; Wolverton, C.; Dravid, V. P.; Kanatzidis, M. G. All-scale hierarchical thermoelectrics: MgTe in PbTe facilitates valence band convergence and suppresses bipolar thermal transport for high performance. *Energy Environ. Sci.* **2013**, *6*, 3346.
(30) Rowe, D. M. *Thermoelectrics Handbook: Macro to Nano*, 1st ed.; CRC Press, Taylor & Francis Group: Boca Raton, FL, 2006.
(31) Bessas, D.; Simon, R. E.; Friese, K.; Koza, M.; Hermann, R. P. Lattice dynamics in intermetallic Mg_2Ge and Mg_2Si. *J. Phys.: Condens. Matter* **2014**, *26*, 485401.
(32) Wang, H.; Jin, H.; Chu, W.; Guo, Y. Thermodynamic properties of Mg_2Si and Mg_2Ge investigated by first principles method. *J. Alloys Compd.* **2010**, *499*, 68−74.

DOI: 10.1021/acsomega.7b01389
ACS Omega 2017, 2, 8069−8074